J. Fluid Mech. (1992), *vol.* 234, *pp.* 171–190
Printed in Great Britain

An experimental investigation on the collision behaviour of hydrocarbon droplets

By Y. J. JIANG, A. UMEMURA AND C. K. LAW
Department of Mechanical and Aerospace Engineering, Princeton University, Princeton, NJ 08544, USA

(Received 13 July 1990 and in revised form 28 May 1991)

The collisional dynamics of equal-sized water and normal-alkane droplets, in the 150 μm radius range, have been experimentally studied for situations involving $O(1)$ droplet Weber numbers and head-on to grazing impact parameters. Results show that in the parametric range investigated the behaviour of hydrocarbon droplets is significantly more complex than that of water droplets. For head-on collisions, while permanent coalescence always results for water droplets, the outcome is quite non-monotonic for the hydrocarbon droplets in that, with increasing droplet Weber number, the collision can result in permanent coalescence, bouncing, permanent coalescence again, and coalescence followed by separation with or without production of satellite droplets. Similar complexities exist for off-centre collisions. Phenomenological explanations are offered for these observations based on the material properties of the fluids, the relative influences of the normal and shearing aspects of the collision, and the nature and extent of energy dissipation due to droplet deformation during collision.

1. Introduction

Recent studies on spray combustion have emphasized the importance of the processes occurring within the dense spray region immediately downstream of the spray injector (Faeth 1977; O'Rourke & Bracco 1980). Here the droplet ensemble is created and its properties serve as the initial conditions for the subsequent development and combustion of the spray. Because of the dense nature of the droplet concentration in this region, it is reasonable to expect that droplet collision is a frequent event. Depending on the velocity and configuration of the impaction, as well as the rheological properties of the fluid, such a collision can lead to various outcomes, such as bouncing, coalescence, and spattering. Thus the initial spray statistics in terms of the number density, size and velocity of the droplets can be significantly affected by droplet collision.

Previous studies on droplet collision have mostly employed water as the medium of investigation because of meteorological interests. Among them are experiments by Adam, Lindblad & Hendricks (1968) for equal-sized droplets in the diameter range from 120 to 1000 μm, Jayaratne & Mason (1964) for different-sized droplets with 300 to 1200 μm diameter, and Bradley & Stow (1978) for different-sized, charged droplets around 1000 μm in diameter. These works typically show results like figure 1, which is taken from Brazier-Smith, Jennings & Latham (1972). That is, permanent droplet coalescence is favoured for small values of the collision Weber number, We, and impact parameter, B, which are respectively defined as (figure 2)

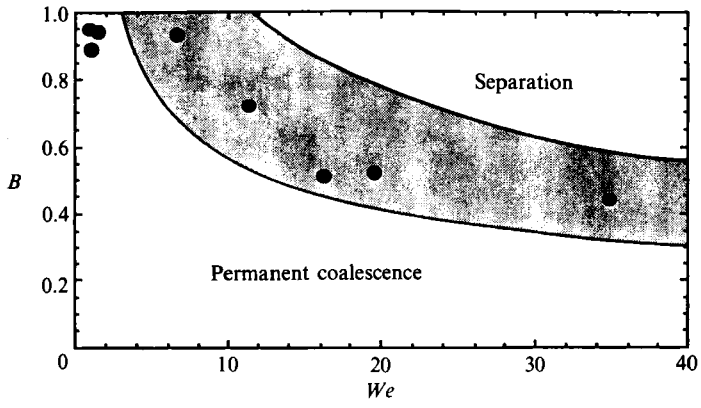

FIGURE 1. The transition boundary for coalescence and separation for water droplet collision. Shaded area represent the band of data of Brazier-Smith *et al.* (1972); solid circles are the present data.

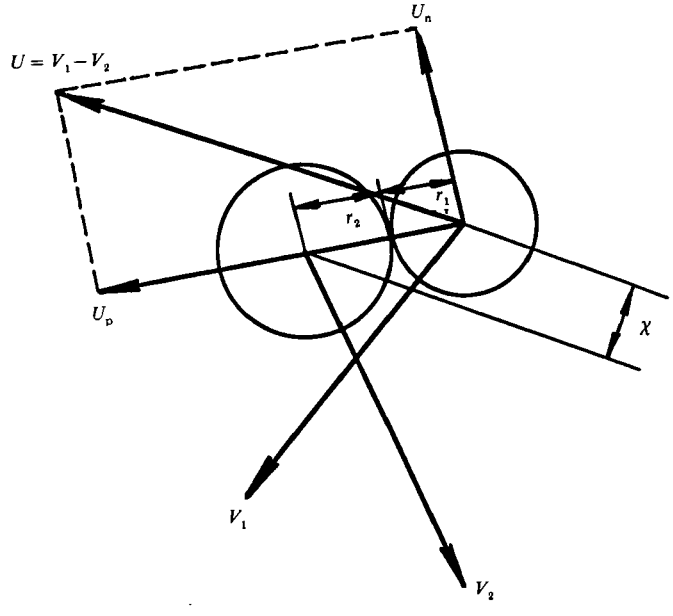

FIGURE 2. Definitions of the various collision parameters at the instant of impact.

$$We = \frac{\rho(r_1 + r_2)\, U^2}{\sigma}, \quad B = \frac{\chi}{r_1 + r_2},$$

where r_1 and r_2 are the radii of the colliding droplets, U the relative velocity at collision, and ρ and σ respectively designate the density and surface tension of the fluid. However, for large values of these parameters, permanent coalescence cannot be achieved. Collision results in either bouncing of the two colliding droplets or their temporary coalescence but eventual separation with or without additional satellite droplet. The boundary of transition monotonically decreases in the (B, We)-plane, as shown in figure 1. The collision of hydrocarbon droplets has been recently studied by Ashgriz & Givi (1987, 1989) and Brenn & Frohn (1989), who used n-hexane and propanol, respectively; the results reported are mainly observational in nature.

In the present investigation we have performed an extensive and systematic study of the collision of droplets of water and hydrocarbons, and have found that the collisional dynamics and outcome for the hydrocarbon droplets can be significantly different from those for the water droplets in the parametric range studied. Of particular interest is the observation that the transition between droplet separation and coalescence for hydrocarbons is far from being monotonic, and so the physical phenomena involved are substantially richer than previously recognized.

In the next two sections we shall present our experimental methodology and data. The data will consist of classifications of the various outcomes of collision, both photographically and in terms of parametric quantification. We shall then present, in §4, interpretations of our observed phenomena.

2. Experimental methodology

A crucial requirement of the present experiment is the generation of spatially and temporally stable droplets over extended periods of time. To meet the requirement of temporal stability, we adopted the ink-jet printing technique (Carnahan & Hou 1975; Wang, Liu & Law 1984) in which a stable stream of droplets of uniform and controllable size and spacing is generated by using a piezoelectric crystal coupled to a glass nozzle. Thus droplet collision can be effected by directing one droplet stream against another with the use of a three-dimensional positioner. The droplet generator can also be rotated in the vertical plane in order to obtain different collision trajectory angles. By, further, observing the collision trajectories vertically downward, the collision is assured to occur in a vertical plane. The droplet image and collision history are recorded on a video recorder by using a strobelight synchronized with the droplet generator with various phase differences. Spatial stability is achieved by isolating the experimental apparatus from the laboratory environment as much as possible.

From the recorded images r_1, r_2 and U can be measured and consequently We and B determined. In the present investigation we are only concerned with the collision between two droplets of the same size, i.e. $r_1 = r_2 \equiv r$. Since it is extremely difficult to generate droplets of identical size from two separate nozzles, we have tried to hold the difference between the two droplet sizes to be less than 10%. Suffice it to note that previous as well as present results both indicate the adequacy of the B–We correlation for droplets of different sizes.

Extensive experiments were performed for distilled water, heptane, decane, dodecane, tetradecane, and hexadecane. The droplet radii for the data reported herein were about 150 μm while the collision Weber numbers ranged approximately up to 100. The values of the viscosity coefficient μ and surface tension σ for the hydrocarbons are given in figure 3 for reference. The corresponding values for water are 1.00×10^{-3} N s/m^2 and 72.9×10^{-3} N/m. It was further found that the water droplets were slightly charged while the hydrocarbon droplets were basically uncharged. The charged nature of the water droplets does not appear to affect the collision behaviour because the present results largely agree with those in the literature obtained through other means of droplet generation, as will be presented next.

Further experimental specifications are given in the Appendix.

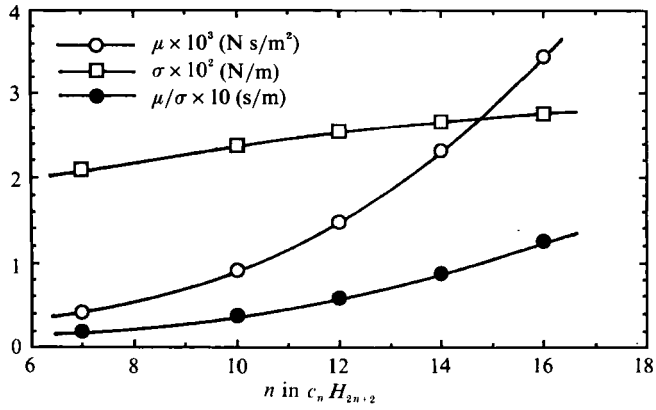

FIGURE 3. Values of the viscosity coefficients and surface tensions of the various normal alkanes, with n being the number of carbon atoms in the molecule.

3. Experimental observations and results

Experiments were first conducted with water droplets in order to validate the present apparatus and procedure against the published results. Figure 1 shows the boundary of permanent coalescence in the B versus We plot for the present data as well as the band of data given by Brazier-Smith *et al.* (1972). The agreement can be considered to be adequate in view of the substantial amount of scatter associated with experiments of this nature.

Figures 4(*a*)–4(*e*) show the corresponding plots for heptane, decane, dodecane, tetradecane and hexadecane respectively. It is clear that the regimes of permanent coalescence for these fuel droplets are quite different from that of water droplets. This behaviour can be approximately classified into five regimes, I to V, as shown in figure 5. Separation of Regimes I to IV is schematically indicated by the solid curves B_a, B_b, and B_c, while Regime V represents high-impact-intensity, grazing collisions. We also define in figure 5 three transition Weber numbers, We_a, We_b, and We_c, to indicate the change in behaviour for the head-on collisions. Figures 6 and 7 respectively show the photographic images of representative collision sequences for the head-on and off-centre collisions. Regime IV is not shown in figure 7 because its behaviour is qualitatively similar to the corresponding situation of figure 6 on account of the small collision parameter B. We also mention that for some of the collision sequences of figures 6 and 7, the photographic images of the droplets which are about to collide, at time = 0, seem to show that the droplets are connected. Such images are deceptive and mostly result from the difficulty in resolving the contrasts in photographic development; the droplets are actually separated at this instant when viewed from the negatives. These imaging difficulties are not to be confused with the experimental observations in the literature (Miller, Sheldon & Atkinson 1965; Santor & Abbott 1968; Ochs & Czys 1987) showing the existence of connecting ligaments for colliding water drops which are either oppositely charged or under the influence of strong electric fields. Such electric forces do not exist for the present experiments.

We first discuss the head-on and near-head-on situations of figure 6. In Regime I the Weber number is not large. Thus the droplets suffer only a moderate amount of deformation upon 'contact'. Disappearance of the interface, however, occurs readily.

In Regime II the collision is sufficiently energetic that substantial droplet deformation occurs. A distinct interface, however, always exists between the

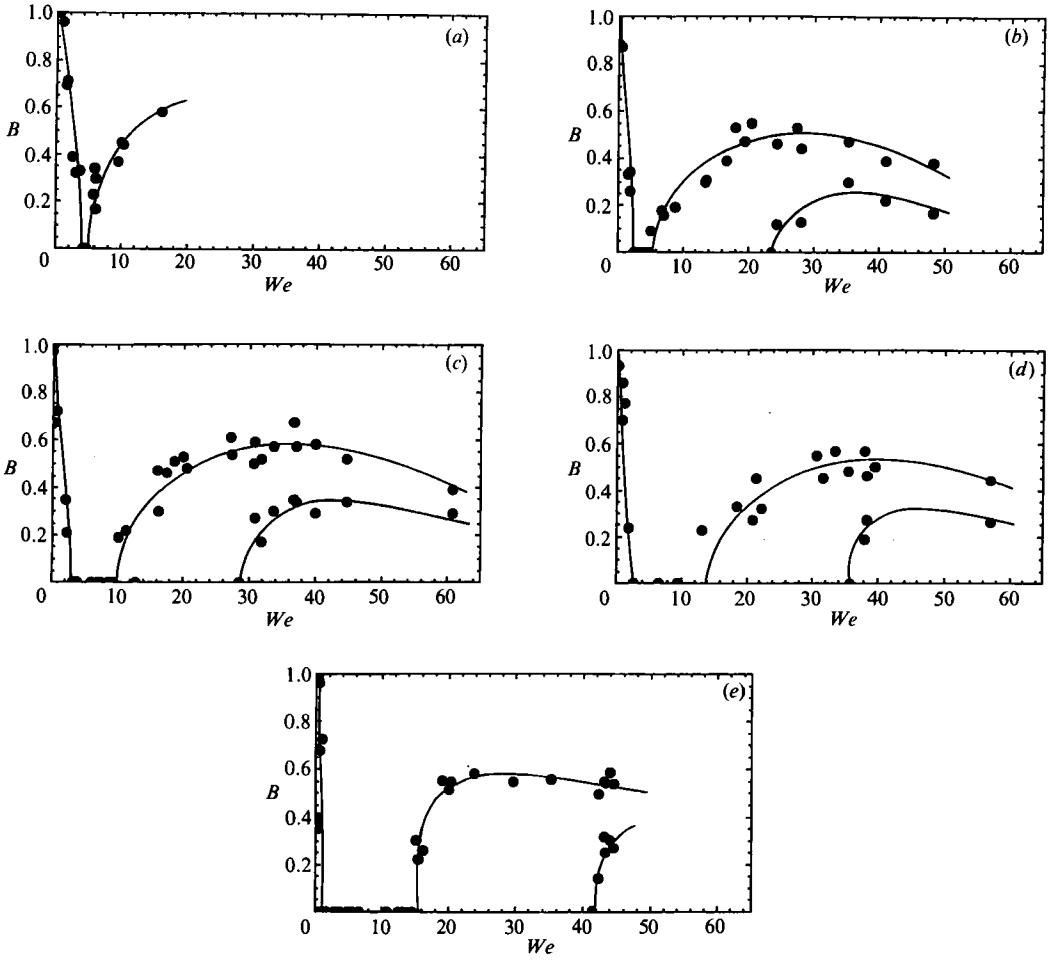

FIGURE 4. Boundaries between coalescence and separation regimes for the various hydrocarbons investigated: (*a*) heptane, C_7H_{16}; (*b*) decane, $C_{10}H_{22}$; (*c*) dodecane, $C_{12}H_{26}$; (*d*) tetradecane, $C_{14}H_{30}$; (*e*) hexadecane, $C_{16}H_{34}$.

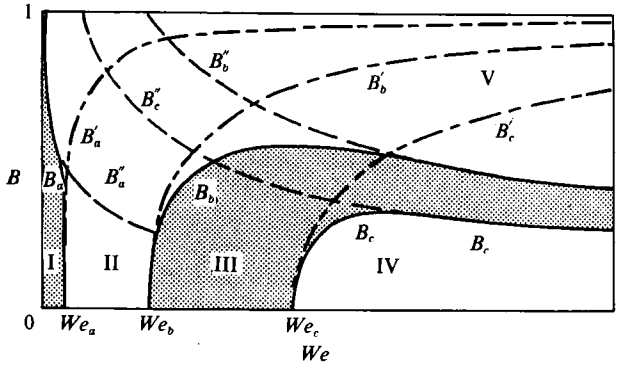

FIGURE 5. Schematic of the various boundaries for coalescence and separation. Solid lines ($B_i, i = a, b, c$) designate the experimental observations. Chain lines (B'_i) designate expressions based on slightly off-centred collision. Dashed lines (B''_i) designate expressions based on grazing collision.

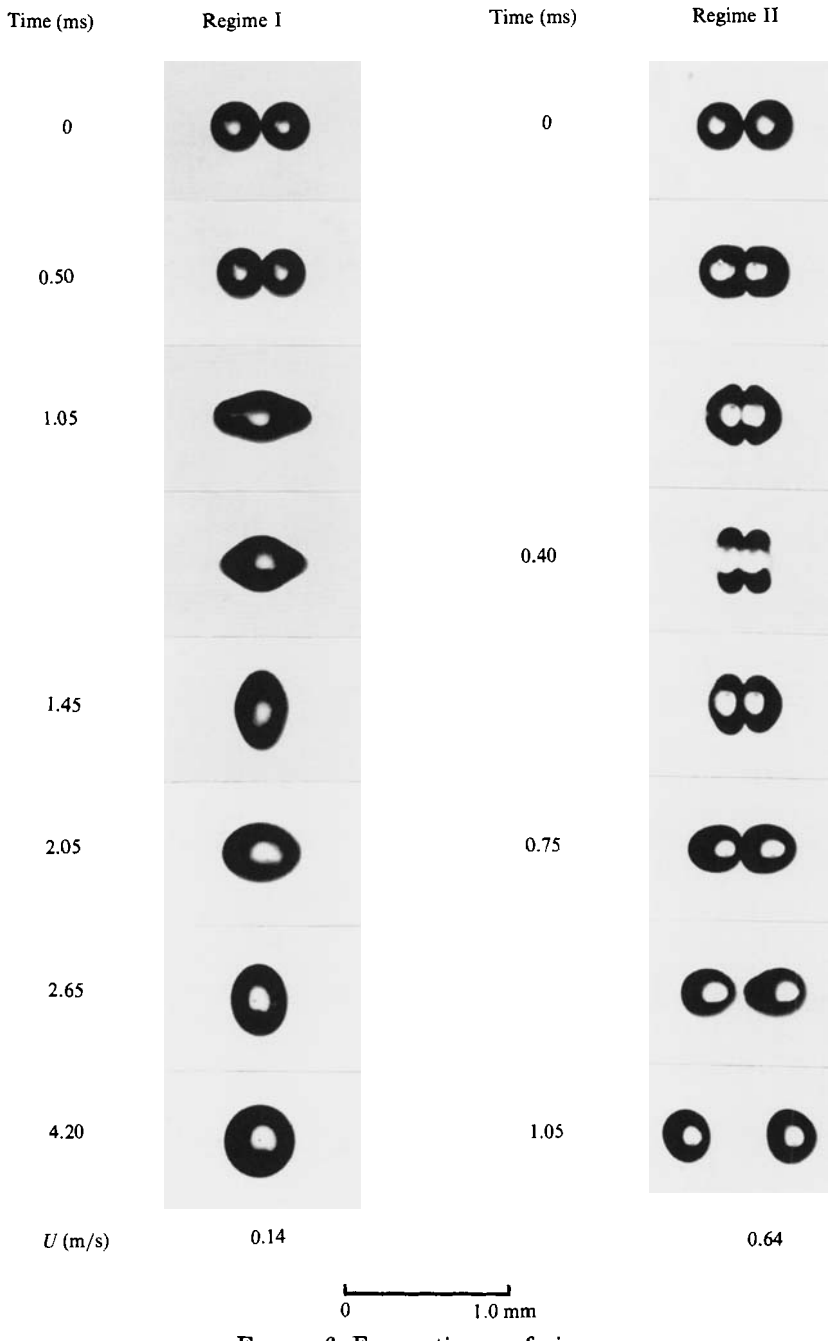

FIGURE 6. For caption see facing page.

droplets as evidenced by the presence of cusps at the edge of the interface. Thus merging does not occur in this regime and the droplets subsequently bounce off.

A further increase in the collision energy results in permanent coalescence, in Regime III, and is characterized by the total deformation of the merged droplet to the shape of a dimpled disc. Finally, in Regime IV, the collision energy is so high that the surface energy of the coalesced mass is not sufficient to contain the liquid in a closed surface. Thus after the initial coalescence, contraction of the deformed droplet

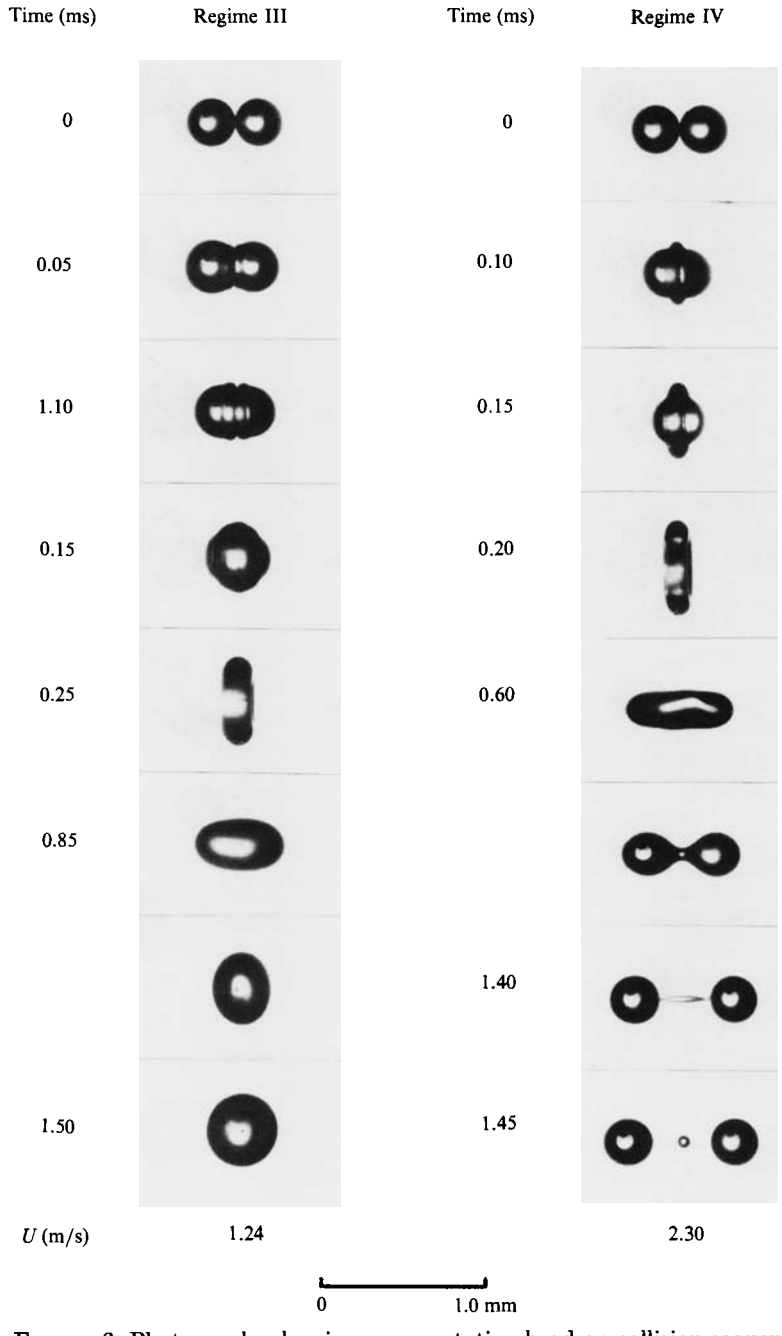

FIGURE 6. Photographs showing representative head-on collision sequences in Regimes I–IV.

causes it to split. The outward velocity of the two receding fragments can cause instability of the ligament connecting them, resulting in the formation of one or more satellite droplets. The number of satellite droplets appears to increase with increasing collision energy.

It is significant to point out again that while permanent coalescence always results for the head-on collision of water droplets in the *We* range investigated (figure 1), for

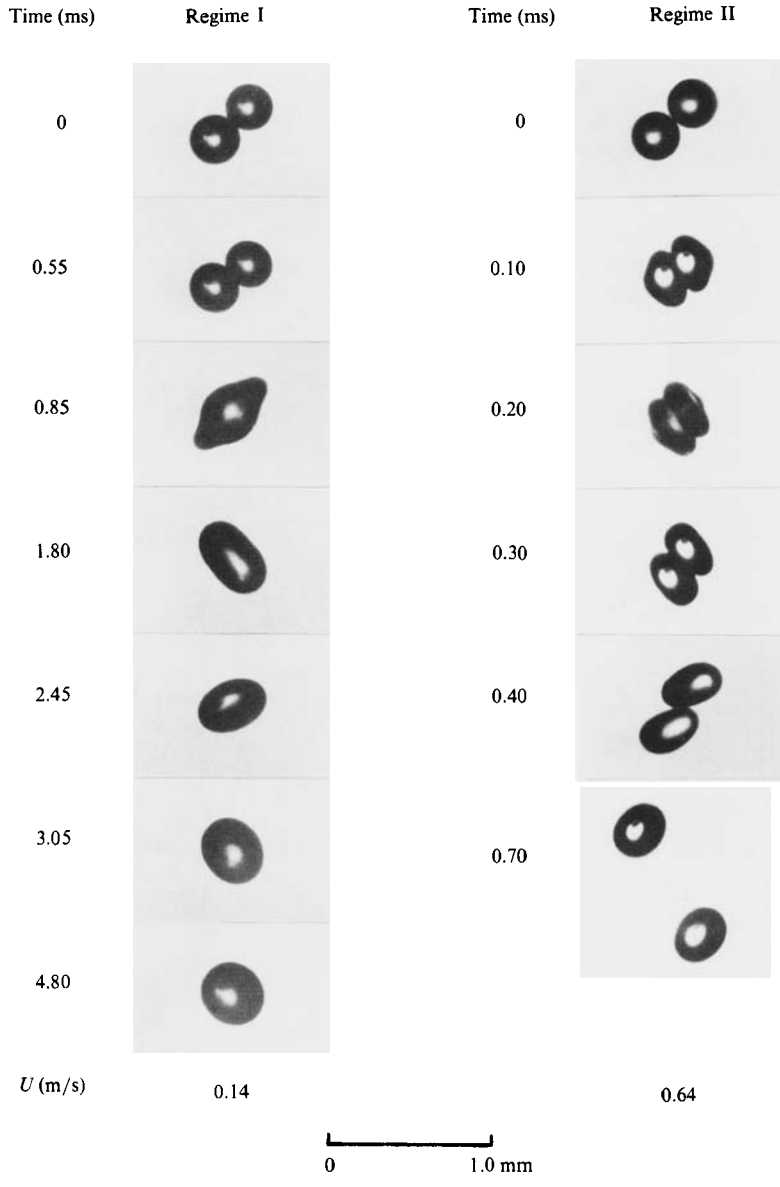

FIGURE 7. For caption see facing page.

the hydrocarbon droplets bouncing and further breakup can also occur. Furthermore, the failure to achieve permanent coalescence does not occur monotonically with increasing collision energy. Thus with increasing collision energy, we have the phenomena of permanent coalescence, bouncing, permanent coalescence again, and coalescence followed by separation accompanied by the possible production of satellite droplets. These differences in the behaviour of water and hydrocarbons are obviously consequences of the differences in their material properties, especially the surface tension as represented by the Weber-number correlation.

For off-centre collisions in Regimes I to IV, the behaviour is qualitatively similar to the corresponding head-on situations except that a rotational motion is now imparted to the droplets in contact. Regime V, however, has some distinctive

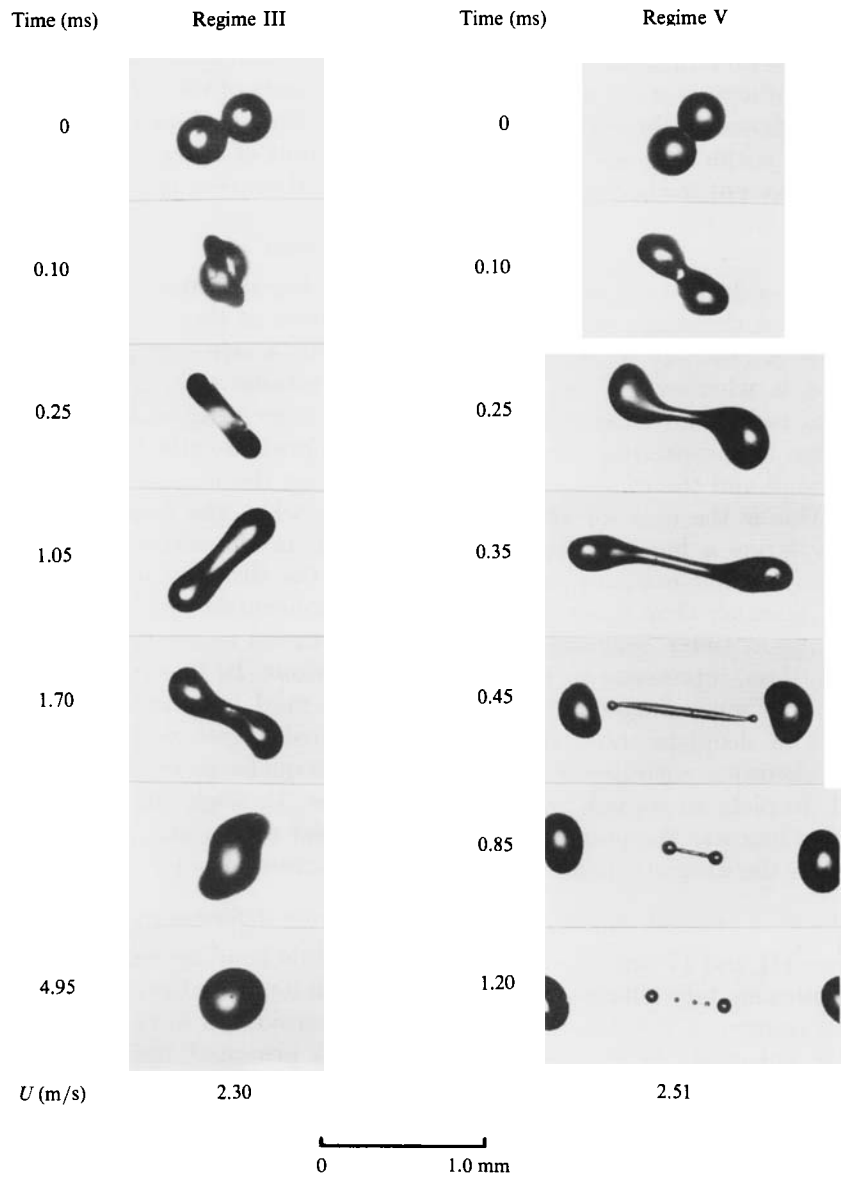

FIGURE 7. Photographs showing representative off-centre collision sequences in Regimes I, II, III, and V.

characteristics. Here collision is grazing and highly energetic. Thus shearing action dominates and there is very little rotational motion. Satellite droplets are produced at higher collision energies and hence Weber numbers.

4. Discussion

A detailed quantitative simulation and prediction of the various phenomena observed would require sophisticated numerical calculation which is beyond the scope of the present investigation. Some useful physical insights, however, can be gained through phenomenological analysis, as will be shown in this section. We are

especially interested in understanding the droplet collisional dynamics in terms of (*a*) the similarities and differences in the collision of water and hydrocarbon droplets, (*b*) the relative influences of the normal and shearing aspects of the collisional dynamics, (*c*) the dependence on the material properties of the fluid such as the surface tension and viscosity coefficient, and (*d*) the nature and extent of energy dissipation during collision. All except the last subsection to be discussed concern head-on or near-head-on collisions.

4.1. *Criteria for coalescence*

Two impacting droplets may coalesce when their clearance reaches a critical value which is within the range of the intermolecular forces of the fluid, typically of the order of 10^2 Å (Mackay & Mason, 1963). Therefore a criterion governing droplet coalescence is whether the minimum clearance attains this critical value. Two possibilities can be envisioned under which such a merging of the interfaces can occur. When the impacting velocity is small, the pressure rise in the interdroplet region is small and the minimum clearance occurs on the line of centres of the two droplets. This is the case for Regime I. However, when the impacting velocity is sufficiently large, a high-pressure field is built up in the direction of the line of centres, causing indentations on the surfaces of the droplets in this region. The minimum clearance then takes the form of a ring concentric with the line of centres (Lee & Hodgson 1968). Regimes III and IV are believed to belong to this category. Regime II, then, represents an intermediate behaviour. In this regime the collision is sufficient to cause flattening and possibly also mild indentations of the facing surfaces. The droplets, however, lose their translational velocities before the minimum clearance distance is reached. The subsequent recovery process for the deformed droplets to resume their spherical shape, through the action of surface tension, will increase the pressure in the interdroplet region and thereby widen the gap between the droplets, resulting in the phenomenon of bouncing.

4.2. *Energy dissipation at maximum deformation*

In Regimes III and IV the two droplets which collide head-on coalesce and deform into an approximately oblate spheroidal shape with its axis of revolution parallel to the line of centres of the droplets. The oblate spheroid can have its centres either bulging or indented. In the experiment the two principal radii, a and b, were measured at the instant when the larger radius, a, became maximum. Assuming an elliptic cross-section, the surface area of the spheroid, S, is given by

$$S = 2\pi a^2\left[1+\frac{1}{\beta(\beta^2-1)^{\frac{1}{2}}}\ln\left(\beta+(\beta^2-1)^{\frac{1}{2}}\right)\right] \quad \text{with} \quad \beta=\frac{a}{b}>1. \tag{1}$$

The total energy of the droplets impacting with speed, $V=\frac{1}{2}U$, is

$$E_0 = 2[(\tfrac{4}{3}\pi r^3)(\tfrac{1}{2}\rho V^2)+\sigma(4\pi r^2)]. \tag{2}$$

From energy conservation, this must be equal to

$$E = \sigma S+\Phi, \tag{3}$$

where σS is the surface energy of the united spheroid, Φ the energy which has been dissipated at the instant under consideration, t, and if we assume all internal motions cease at this instant. The dissipation energy Φ is given by

$$\Phi = \mu\int_0^t \mathrm{d}t\int\frac{1}{2}\left[\frac{\partial v_i}{\partial x_j}+\frac{\partial v_j}{\partial x_i}\right]^2(\mathrm{d}x)^3, \tag{4}$$

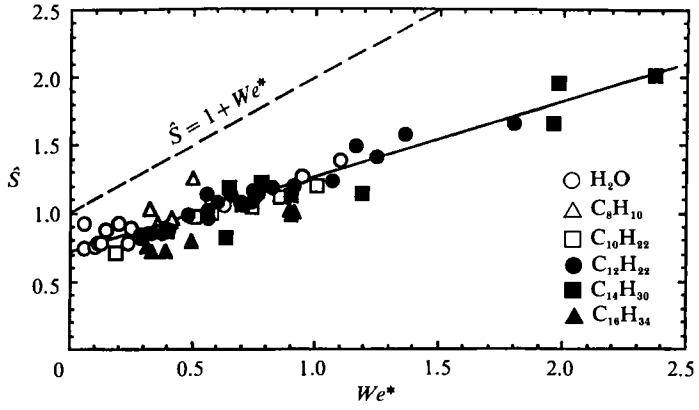

FIGURE 8. Variation of $\hat{S}$ with We^* for the assessment of viscous loss during droplet deformation. Symbols are experimental data and the solid line their correlation. Dashed line is theoretical expression assuming no loss.

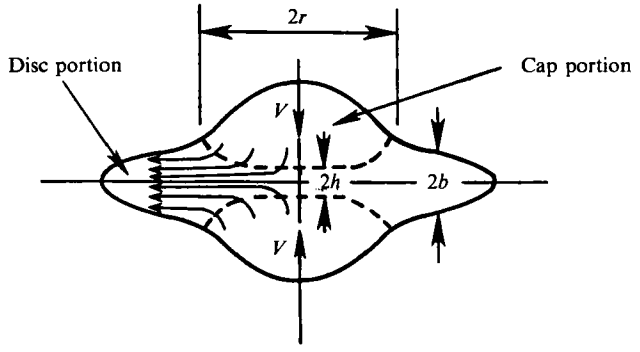

FIGURE 9. Schematic of the model adopted in analysing the droplet deformation and viscous loss processes.

provided that the work on the surrounding gas by the droplet is negligible in comparison with the viscous dissipation within the droplet. The integration over $(\mathrm{d}x)^3$ in (4) is to be performed over the droplet volume. In writing (3) we have also assumed that the flow within the united spheroid stagnates at the instant of maximum deformation. Equating (2) and (3) we have the following relation:

$$\hat{S} = 1+(1-\alpha)\,We^*, \tag{5}$$

where $\hat{S} = S/8\pi r^2$ and we have also defined a droplet Weber number as $We^* = \rho r V^2/6\sigma$ such that $We^* = We/48$. The quantity αWe^* corresponds to the dissipation energy Φ in the non-dimensional form so that α can be called a dissipation coefficient.

In figure 8 the quantity $\hat{S}$, calculated from the measured values of a and b, is plotted against We^* for the various materials tested. All data appear well correlated with a single straight line. A comparison to the dashed line given by (5) with $\alpha = 0$ shows that about half of the initial kinetic energy is lost in the deformation process.

We next consider in more detail the process of energy dissipation during collision. Figure 9 shows a schematic of a typical collision configuration, after coalescence but before the maximum deformation. The configuration can be considered to consist of two end caps sandwiching a central disc. For simplicity it is reasonable to assume

that the end caps are minimally affected by the collision such that they translate at the original velocity V and retain the spherical contour of the original droplets. These impacting masses serve as impinging jets in the formation of the outwardly spreading fluid disc. Therefore, the time which lapses until the droplet reaches its maximum deformation can be estimated to be of the order of $2r/V$. The thickness $2h$ of the stagnation flow region, which is formed on the central plane by the impinging flow, can be determined by first noting that the maximum velocity gradient exists in the stagnation flow region and the order of magnitude of the strain rate is V/h. By further using the relation $\frac{1}{2}\rho V^2 \sim \mu V/h$, we get $h \sim 2\mu/\rho V$. Since the volume of this stagnation flow region is of the order of $(2h)(\pi r^2)$, the amount of energy dissipation in this region, according to (4), is

$$\Phi \sim \mu[V/h]^2 (2\pi h r^2)[2r/V] \sim 2\pi\rho r^3 V^2. \tag{6}$$

The above relation shows the interesting result that the amount of viscous energy dissipation is independent of the viscosity coefficient μ. This result is consistent with the experimental data of figure 8, which show that Φ is proportional to We^* but does not depend on μ explicitly. That is, since the present data include materials whose viscosities range from 0.907×10^{-3} to 3.45×10^{-3} N s/m^2, significant changes in slope would have been observed for different materials if Φ depended on μ explicitly. The final point to note is that the above estimate of viscous loss includes only considerations in the stagnation region of the disc but not the amount in the spreading rim region. It is reasonable to assume that the amount of energy dissipation in this region is small, especially for large values of V, because the free surface can adjust the flow to lessen the velocity gradients there.

We next study the properties of the rim region of the disc. The pressure at the rim is of the order σ/b, which should be balanced by the stagnation pressure, $\frac{1}{2}\rho V^2$, in the course of developing the disc. This can be established by noting that during the initial period of coalescence, the stagnation pressure far exceeds the surface tension pressure. This leads to an outwardly accelerating radial flow which reduces the width of the disk and increases the pressure at the rim in an attempt to balance the stagnation pressure. By the same reasoning, when the rim pressure exceeds the stagnation pressure in the final stage of deformation, development of the disc ceases and the disc will contract back. Balancing the two pressures yields

$$\frac{b}{r} \sim \frac{\sigma}{\frac{1}{2}\rho r V^2} \sim \frac{1}{3We^*}, \tag{7}$$

which takes a value of order unity in the range of We^* tested, and agrees with the experimental observation (see, for example, figure 6).

The above arguments are made based on the asymptotic feature of large V. A consistency check can also be performed. That is, combining the a^2 expression given by (5), in the limit of large β, and the b expression of (7), yields

$$a^2 b \sim r^3, \tag{8}$$

which is a statement of mass conservation in that the initial mass of the colliding droplets is of the same order as the resulting mass of the coalesced droplet, and that this relation is independent of the other system parameters such as σ, μ, and V.

There are two additional comments. First, because of inertia the fluid in the disc portion continues to move outward even after the cap portions are exhausted. This is why we sometimes see indentations at the central part of the united spheroid at

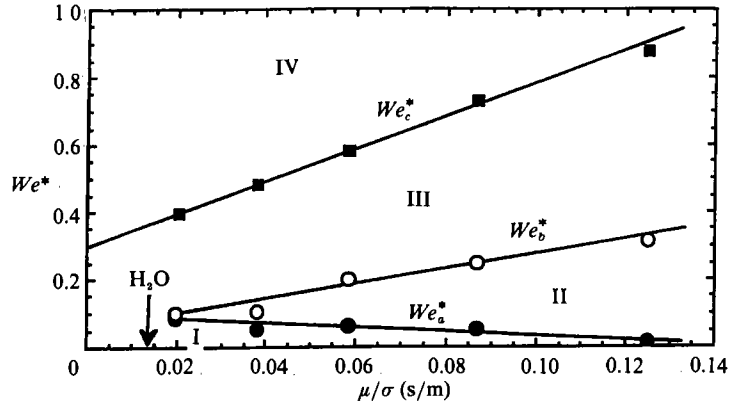

FIGURE 10. Correlation of the transition Weber numbers with μ/σ.

the maximum deformation. If the impacting velocity is much higher than the present ones, the central portion of the disc would be thinner which could lead to instability and consequently droplet splitting at the maximum deformation stage (Adam *et al.* 1968). Second, our discussion in this section is mainly concerned with relatively large impact velocities as indicated by the linearity in the plot of figure 8. For smaller impact velocities, caution should be exercised in utilizing the present results and insights. In particular the plots in figure 8 do not include data for Regime I because of the small values of We^*.

4.3. *Characteristics of transition Weber numbers*

Interesting information can be obtained by examining the critical Weber numbers of transition for head-on collisions, We_a, We_b, and We_c in figure 5. We first consider We_c, which is the transition state at which the coalesced droplet either remains permanently united or separates into several droplet fragments. Figure 10 shows that We_c^* varies linearly with μ/σ for all of the hydrocarbons tested. Since the values of σ for these hydrocarbons do not vary much from each other, as shown in figure 3, the result of figure 10 basically demonstrates that We_c^* varies linearly with μ.

To gain insight into the above behaviour, we first note that around the transition state the centre of mass of the droplets after collision should have no velocity except that due to the effect of gravity. Therefore, if separation does not occur, then the coalesced droplet will oscillate about its equilibrium state of a sphere of radius $2^{\frac{1}{3}}r$, and eventually dissipates the excess surface energy. On the other hand, if separation occurs, then by symmetry the coalesced droplet should be split into two secondary droplets without any overall translational energy but with some excess energy which is again to be dissipated through oscillation. In either case we can equate the initial energy given by (2) to the final surface energy plus all of the dissipated energies. In non-dimensional form such a statement of energy conservation can be expressed as,

$$We_c^* + 1 = 2^{-\frac{1}{3}} + \Phi_{\mathrm{III}}/8\pi r^2\sigma = 1 + \Phi_{\mathrm{IV}}/8\pi r^2\sigma, \tag{9}$$

where Φ_{III} and Φ_{IV} respectively denote the total amount of energy dissipated as a result of collision in Regimes III and IV. Phenomenologically, droplet energy dissipation can be considered to occur in two distinct phases. The first is characterized by significant droplet distortion which is rapidly damped out. The energy dissipation in this phase is independent of viscosity, as was demonstrated in relation to the discussion of figure 9. The second phase occurs during the small-amplitude free

oscillation of the droplet(s) through surface tension forces. Since according to the linear theory of free oscillation the period of oscillation is proportional to $r(\rho r/\sigma)^{\frac{1}{2}}$, the energy dissipated during this motion is of the order of $\mu(\sigma/\rho r)^{\frac{1}{2}}r^2$, or $(\mu/\sigma)(\sigma/\rho r)^{\frac{1}{2}}$ in non-dimensional form. Adding the energy dissipation from these two phases, (9) can be expressed as

$$We_c^* = K(\mu/\sigma) + C, \tag{10}$$

where K and C are independent of μ. Equation (10), of course, is in the same form as the experimental results for We_c^* of figure 10, thereby substantiating our interpretation of the dissipation processes during droplet collision. It may also be noted that the intersection point of the We_c^* line with the vertical axis gives the energy which the separated droplets have in the form of oscillatory motion to be eventually dissipated.

Figure 10 shows that the critical Weber number, We_b^*, for the transition between Regimes II and III also increases linearly with μ. This suggests that although the degree of deformation is reduced here as compared to the We_c^* transition, the energy dissipation processes are probably similar. A major difference here is the existence of an intervening gas film in Regime II. It is, however, reasonable to expect that as long as V is relatively large, this gas film of small viscosity offers little resistance to the radial liquid flow caused by the impacting droplet caps and therefore should not have much influence on the degree of droplet deformation.

However, with continuous decrease in the impact velocity, the effect of the gas film eventually becomes significant enough to control droplet deformation, as evidenced by the distinct property of We_a^* which is a decreasing function of μ/σ. Since the phenomenon in this situation is not easy to explore without detailed analysis, we only mention the following interesting observation shown in figure 10. It is seen that the two critical curves of We_a^* and We_b^* merge at the small value of $\mu/\sigma = 0.02$ s/m, suggesting that bouncing of the droplets does not occur for materials with μ/σ smaller than this value under the same experimental conditions in terms of, say, the droplet size and the air environment. Since water has $\mu/\sigma = 0.014$ s/m, which is smaller than the limiting value identified, it is then reasonable that, in previous (Brazier-Smith *et al.* 1972) as well as the present experiments with water, bouncing of the droplets was not observed for head-on and near-head-on collisions. To further substantiate this possibility, we have experimented with xylene whose μ/σ is near the limiting value. In this case the collision/coalescence behaviour is very unstable in that the collision regimes change even in the presence of small disturbances. This also suggests that this limiting point could indeed be a controlling factor in the coalescence of head-on collisions. We note that in past studies little attention has been paid to the effects of the rheological properties of the fluid under investigation. The present results suggest their potential importance which warrants further study.

We finally discuss the role of σ in the representation of figure 10. While we have selected μ/σ as the abscissa in order to cover all regimes in as unified a way as possible, it is easy to see that the appropriate non-dimensional quantities involving μ are different for large and small values of V. For large V the phenomenon is characterized by the prominence of the impinging flow region. As seen from the derivation of (10) the appropriate non-dimensional quantity in this case is $(\mu/\sigma)(\sigma/\rho r)^{\frac{1}{2}}$, although in the range of our experiments the factor $(\sigma/\rho r)^{\frac{1}{2}}$ does not change significantly. On the other hand, for small V the quantity μ/σ should be non-dimensionalized in terms of V because droplet deformation in Regimes I and II is strongly influenced by the gas film between the droplets. Therefore, for fixed V and μ we may expect that a material with large σ, as in the case of water, is more likely

to coalesce because of the greater amount of the surface energy. This therefore implies the existence of a lower bound in μ/σ for Regime II.

4.4. *Characteristics of off-centre collisions*

We now consider the boundary curves of figure 5 for off-centre collisions characterized by $B > 0$. From figure 2 the impacting droplet velocity components parallel and normal to the line of centres are given by $U_p = U(1-B^2)^{\frac{1}{2}}$ and $U_n = UB$, respectively. For small values of B the collision process is dominated by the longitudinal velocity component U_p while the transverse velocity component U_n can have at most a minor effect, of the order of B, on the accompanying droplet deformation. We therefore expect that almost the same collision process takes place for the same value of U_p, such that for slightly, or perhaps even moderately, off-centre collisions the boundary lines are given by

$$B_i'(We) = \left(1-\frac{We_i}{We}\right)^{\frac{1}{2}}, \quad i = a, b, c. \tag{11}$$

These are given by the chain lines originating at We_i in figure 5.

As B becomes greater the effect of the transverse velocity component U_n becomes significant, so that the real boundary curves deviate from (11) gradually. For the boundary of Regime I, the deformation of droplets upon collision is relatively small because of the small Weber number. To the left-hand side of the curve B_a' of (11) the droplets have a chance to coalesce permanently. However, the critical curve does not describe centrifugal forces exerted by the transverse velocity components ($\frac{1}{2}U_p$) tending to break the bridging between the droplets. This break will occur if the centrifugal force exceeds the bonding force by surface tension at the bridged part. Assuming a constant bonding force F, we have another critical condition,

$$F \sim \rho(\tfrac{4}{3}\pi r^3)\frac{(\frac{1}{2}U_p)^2}{r} \quad \text{or} \quad B_a'' \sim \frac{1}{We^{\frac{1}{2}}}, \tag{12}$$

which gives the curve B_a'' in figure 5. On the right-hand side of this curve the bridging may break. That is, the boundary of Regime I is switched from the curve B_a' to B_a'' at a moderate B-value. As the Weber number is increased to overcome the resisting gap pressure, the droplets again coalesce with large deformation upon collision.

According to our observation the effect of U_n appears in the form of a sliding motion of the original droplet masses such that separation of the merged mass in, say, Regime III is caused by this overwhelming shearing process. To understand this phenomenon let us first consider the following. During the initial stage it is mainly U_p that causes coalescence and deformation into the plate shape. As this deformation reaches the maximum state and the kinetic energy pertaining to the longitudinal velocity U_p is changed into surface energy, the competition between the restoring force from surface tension and the inertial force from U_n then becomes the dominant process. That is, the surface tension tends to make the united mass spherical while the transverse velocity continuously tends to elongate it. Thus, we may expect that the two different effects of U_p and U_n appear in turn without strong interaction between them. In other words, the collision consists of two processes: the initial impacting process leading to the maximum deformation of the united mass in a manner similar to the case of head-on collision, which is followed by the competition between surface tension and the inertia force of the transverse velocity. Splitting occurs when the transverse velocity is large enough.

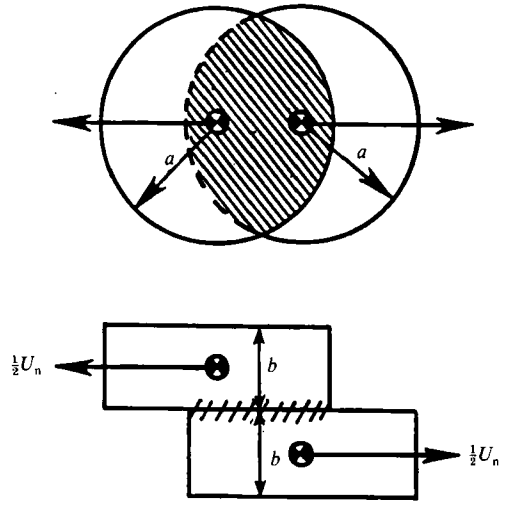

FIGURE 11. Schematic showing the model adopted to analyse droplet breakup during grazing collision by approximating the process as the sliding motion of a merged droplet under the influence of transverse inertia force and restoring surface tension force.

Having recognized that it is U_n which is responsible for droplet splitting, we adopt the model of figure 11 to explain this phenomenon. Here two circular plates in sliding motion at velocity U_n represent the two droplets which are united and are deformed by the longitudinal velocity U_p. There are two major factors which resist their sliding motion. One is the surface tension acting at the circumference, F, whose magnitude is estimated as

$$F \sim (\sigma/b)\,(ab). \tag{13}$$

The other is the viscous force D due to the shearing flow layer between the sliding masses, estimated as

$$D \sim \mu U_n r. \tag{14}$$

Applying the momentum theory for each sliding mass, we have

$$\rho(\tfrac{4}{3}\pi r^3)\,U_n = \int_0^\tau (F+D)\,\mathrm{d}t \tag{15}$$

for the critical situation marking the upper boundary part of Regime III. Since the time, τ, in which the two masses are united, is estimated as $\tau \sim r/U_n$, (15) becomes, in the non-dimensional form,

$$We^{\frac{1}{2}} \sim \frac{1}{B_b''}\left[1+k\frac{\mu}{\sigma}\left(\frac{\rho r}{\sigma}\right)^{\frac{1}{2}}\right], \tag{16}$$

where k is a constant. Above the curve B_b'' in figure 5 the temporally united mass separates again. It is interesting to note that according to (16) the height of the boundary curve B_b'' increases with the fuel viscosity or the number of carbon atoms. This is consistent with our experimental data as seen in figure 4. Taking into account figures 1 and 10 we may conjecture that the two pairs of curves, B_a' and B_b', B_a'' and B_b'', approach and merge with decreasing viscosity-to-surface tension ratio, yielding a boundary curve similar to the water case. This needs to be substantiated by further experiments. Combining the shearing-dominated result of (16) and the impact-

dominated, head-on or near-head-on result of (11), we have the experimentally-observed solid boundary curve of B_b shown in figure 5. The contribution of the viscous force tends to increase the values of B in proportion to μ/σ.

Expression (16) with $k = 0$ is in the same form as that of Brazier-Smith *et al.* (1972), who obtained their criterion based on a balance between the droplet rotational and surface tension forces. This similarity is, strictly, a coincidence because their postulated separation mechanism is completely different from ours. It seems, however, reasonable to suggest that the criterion of Brazier-Smith *et al.* (1972) might not be adequate to explain the separation phenomenon as observed. This is because their configuration of the merged, rotating, reasonably spherical droplet exists only for near-head-on collisions which, however, are described by (11) instead of (16). Furthermore, for the highly off-centre collisions described by (16), the merged liquid mass completely fails to resemble a sphere.

We finally note that the critical curve B_c has a similar form to the critical curve B_b. The existence of this critical curve indicates that the transverse velocity U_n acts to weaken the deformation by U_p that leads to droplet splitting by the longitudinal droplet vibration mode. The same reasoning employed to characterize the critical curve B_b applies to this case as well. That is, with increasing B the competition between the shearing effect of U_n and the surface tension effect becomes the key factor in determining the subsequent processes. For the B_b transition, the shearing effect overwhelms the surface tension effect if we increase B at a fixed We. For the B_c transition, surface tension overwhelms shearing. Apparently the breakdown of axisymmetry due to U_n makes the subsequent longitudinal vibrational motion less effective in disrupting the droplet. This is possibly because the elliptic deformation of the droplet within a plane perpendicular to the centreline is considered to trigger transverse vibration within the plane which is at a lower level in energy.

5. Concluding remarks

The present investigation has revealed several interesting aspects of the collision of droplets of water and n-alkanes. First we have observed that while permanent coalescence always occurs for the head-on and near head-on collisions of water droplets, for the hydrocarbon droplets the collision can result in coalescence, bouncing, coalescence again, and coalescence followed by separation as the collision energy is increased. The difference in behaviour is obviously caused by the difference in the rheological properties of the fluids, especially the surface tension and the viscosity coefficient. Both these parameters, together with the droplet dynamics, control the extents of droplet deformation, viscous loss during the deformation, pressure rise in the inter-droplet spacing, and consequently closest distance the droplets can approach each other. Coalescence is possible when this clearance distance is smaller than a certain critical value which is expected to depend on the material properties of the fluid and the environment. Coalescence also does not imply permanent coalescence because splitting of the merged mass can occur, depending on the surface tension of the material and the amount of the kinetic and surface energies contained within the merged mass.

The fact that water behaves differently from hydrocarbons can thus be interpreted on the basis that, for head-on or near head-on collisions, Regimes II and IV fail to exist for water, at least for the range of parameters investigated. The omission of Regime II, and hence the direct transition from Regime I to Regime III, is then a consequence of insufficient pressure build-up in the inter-droplet spacing such that

the droplets can always approach each other to a distance smaller than the critical clearance value. The omission of Regime IV is due to the insufficient kinetic and surface energies contained within the merged water droplet to make splitting possible. The identification of the special value of $\mu/\sigma = 0.02$ s/m, at which the critical curves of We_a and We_b cross and below which bouncing does not occur, is interesting and merits further investigation.

In the present study we have also demonstrated that droplet energy dissipation could be considered to occur in two phases. The first phase is associated with significant droplet distortion and the amount of energy dissipation is independent of the viscosity coefficient. The second phase is associated with small-amplitude free oscillation of the droplet, and does depend on the viscosity coefficient.

Finally, for sufficiently off-centre collisions, we have suggested that the controlling consideration in the splitting of the merged droplet is the relative intensities of the shearing force versus the surface tension force. This is different from the explanation of Brazier-Smith *et al.* (1972), which is based on the competition between rotational inertia and surface tension force.

This research was supported by the US Air Force Office of Scientific Research and by the Heat Transfer Program of the US National Science Foundation. Professor C. H. Wang, now of the National Taiwan University, contributed the initial design of the apparatus.

Appendix. Further experimental specifications

Figure 12 shows a schematic of the experimental apparatus. Here two identical peizoelectric droplet generators (1) were driven by the pulses from a voltage generator (2) which had two output channels. Each of these channels had independent controls for voltage and pulse width, shared common control for frequency, and one of them had a variable pulse delay. A synchronous single or double pulse with variable delay controls the strobelight (3). In most runs the pulse voltage was varied between 5 and over 100 V. The diameter of the glass nozzles for the droplet generators was the primary parameter in controlling the droplet size, and had been varied from 50 to 300 μm in the experimentation. Typically, the droplet diameter was about twice the nozzle diameter. In order to obtain the desired droplet size and speed, careful matching between the width and amplitude of the pulse, as well as the diameter of the nozzle, was needed. The droplet generators could also rotate in the vertical plane in order to change the trajectory angles of the droplet streams, while precise aiming was accomplished through adjustment of a three-dimensional positioner (4) attached to one of the droplet generators.

The strobelight was aligned with the video camera (5), allowing imaging of the collision even with a system magnification factor of 64. For taking photographs, a magnification factor of about 15 was used. The strobelight was operated in two modes: an independently controlled mode and a mode synchronized with the pulse generator. By using the independently controlled mode, the frequency difference between strobing and droplet generation produced a droplet train which allowed global visualization of the collision event as well as determination of the trajectory angles of the two droplet streams. With the synchronized mode, the droplet image was frozen and its size and shape could be determined. By further applying a double pulse, double images of droplets about to collide were taken, from which the instantaneous velocities of the droplets could be determined.

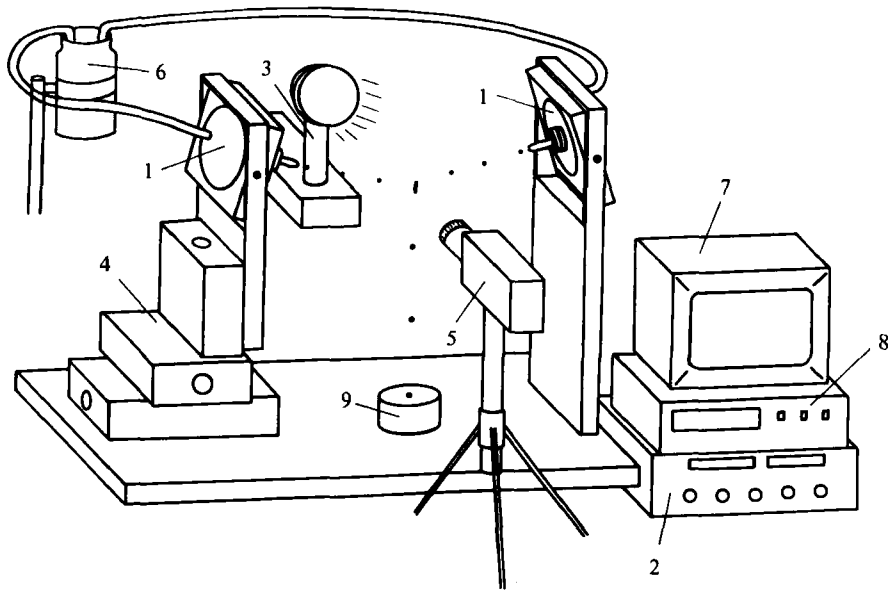

FIGURE 12. Schematic of the experimental apparatus: 1, droplet generator; 2, voltage generator; 3, strobelight; 4, three-dimensional positioner; 5, video camera; 6, liquid reservoir; 7, TV monitor; 8, video recorder; 9, droplet collector.

The level of the test liquid in reservoir (6) was maintained to be at about the same level as that of the nozzle. In order to achieve steady droplet streams, it was also necessary to ensure that all air bubbles were expelled from the droplet generators and the connecting tubing.

REFERENCES

ADAM, J. R., LINDBLAD, N. R. & HENDRICKS, C. D. 1968 The collision, coalescence, and disruption of water droplets. *J. Appl. Phys.* **39**, 5173.

ASHGRIZ, N. & GIVI, P. 1987 Binary collision dynamics of fuel droplets. *Intl J. Heat Fluid Flow* **8**, 205.

ASHGRIZ, N. & GIVI, P. 1989 Coalescence efficiencies of fuel droplets in binary collisions. *Intl Commun. Heat Mass Transfer* **16**, 11.

BRADLEY, S. G. & STOW, C. D. 1978 Collisions between liquid drops. *Phil. Trans. R. Soc. Lond.* A**287**, 635.

BRAZIER-SMITH, P. R., JENNINGS, S. G. & LATHAM, J. 1972 The interaction of falling water drops: coalescence. *Proc. R. Soc. Lond.* A**326**, 393.

BRENN, G. & FROHN, A. 1989 Collision and merging of two equal droplets of propanol. *Exp. Fluids* **7**, 441.

CARNAHAN, R. D. & HOU, S. L. 1975 *Proc. IEEE/IAS 10th Annual Meeting.*

FAETH, G. M. 1977 Current status of droplet and liquid combustion. *Prog. Energy Combust. Sci.* **3**, 191.

JAYARATNE, O. W. & MASON, B. J. 1964 The coalescence and bouncing of water drops at an air/water interface. *Proc. R. Soc. Lond.* A**280**, 545.

LEE, J. C. & HODSON, T. D. 1968 Film flow and coalescence – I. basic relations, film shape and criteria for interface mobility. *Chem. Engng Sci.* **23**, 1375.

MACKAY, G. D. M. & MASON, S. G. 1963 The gravity approach and coalescence of fluid drops at liquid interfaces. *Can. J. Chem. Engng* **41**, 203.

MILLER, A. H., SHELDON, C. E. & ATKINSON, W. R. 1965 Spectral study of the luminosity produced during coalescence of oppositely charged falling water drops. *Phys. Fluids* **8**, 1921.

OCHS, H. T. & CZYS, R. R. 1987 Charge effects on the coalescence of water drops in free fall. *Nature* **327**, 606.

O'ROURKE, P. J. & BRACCO, F. V. 1980 Modelling of droplet interactions in thick sprays and a comparison with experiments. *Stratified Charge Auto. Engng Conf.*, pp. 101–116. Inst. Mech. Engng Pub. ISBN. 0-85298-4693.

SANTOR, J. D. & ABBOTT, C. E. 1968 Charge transfer between uncharged water drops in free fall in an electric field. *J. Geophys. Res.* **73**, 6415.

WANG, C. H., LIU, X. Q. & LAW, C. K. 1984 Combustion and microexplosion of freely-falling multicomponent droplets. *Combust. Flame* **56**, 175.